RSC Advances

PAPER

View Article Online
View Journal | View Issue

Cite this: *RSC Adv.*, 2017, **7**, 704

Ni–reduced graphene oxide composite cathodes with new hierarchical morphologies for electrocatalytic hydrogen generation in alkaline media†

Zhouhao Chen,‡[ab] Lixin Wang,‡[ab] Zhipeng Ma,[a] Jianjun Song[a] and Guangjie Shao*[ab]

Received 10th October 2016
Accepted 14th November 2016

DOI: 10.1039/c6ra24993k

www.rsc.org/advances

Ni–reduced graphene oxide (rGO) composite cathodes were successfully prepared by composite electrodeposition under supergravity fields. The synthesized composite cathodes exhibit unique hierarchical structure with large numbers of Ni nanoparticles anchoring on the rGO surface. Specifically, the sample prepared from the electrolyte containing 0.7 g L^{-1} GO at rotational speed 3000 rpm displays a favorable activity toward the hydrogen evolution reaction (HER) in 1 M NaOH solution with a high exchange current density of 741.3 μA cm^{-2} and a low Tafel slope of 120 mV dec^{-1}. Electrochemical impedance spectroscopy (EIS) and cyclic voltammetric (CV) tests demonstrate that the superior catalytic activity should be ascribed to the enhanced active surface area and the improved intrinsic activity. Furthermore, the morphology and microstructure properties of Ni–rGO cathodes synthesized from various GO concentrations and supergravity fields are systematically investigated.

1. Introduction

Hydrogen, as a clean and sustainable chemical fuel, is recognized as the most promising substitute for fossil fuel in the future energy infrastructure.[1–3] Water electrolysis is a renewable and secure way to create hydrogen of high purity with zero pollutants emission.[4,5] Currently, the state-of-art cathode materials for the hydrogen evolution reaction (HER) are based on Pt and Pt-based materials,[6,7] but their broad applications are restricted by the high cost and resource scarcity. Thus, it is a crucial task to develop effective earth-abundant HER electrocatalysts to replace the precious metals. Among the non-noble metals, Ni and Ni-based electrode materials have been widely considered as promising electrocatalytic materials due to their comparatively large electrocatalytic activity and good stability for HER in alkaline solutions.[8] Two main approaches including alloying Ni with some other metals or non-metals[9–16] and compositing Ni with active nano-sized particles[17–22] have been taken to enhance the intrinsic activity and/or increase the real surface area of electrode materials for HER.

Graphene as a kind of flat sheet comprised of sp^2-hybridized carbon atoms with a two-dimensional (2D) hexagonal honeycomb lattice has received tremendous interests in the electrochemical fields owing to its outstanding chemical and physical properties. For instance, numerous researchers have been devoted to studying the application of graphene/reduced graphene oxide (rGO) in H_2 storage,[23–26] and have found that graphene/rGO could enhance the catalytic activity of metal catalysts through H spillover effect which essentially involves the transfer of dissociated H from a metal catalyst to the graphene substrate. This H spillover effect has also been confirmed to be effective for application in HER electrocatalysis due to the promotion of forming more free active sites on the catalyst surface.[27] Inspired by this result, the synergetic effect would be essential in Ni–rGO composite cathodes to further enhance the electrocatalytic performance of cathodes for HER in alkaline solution.

Generally, the normal electrodeposition is one of the most popular methods to prepare Ni-based-rGO composite coatings by dispersing GO/rGO into electrolyte.[28,29] However, the slow mass transfer and poor by-product bubble separation often lead to low efficiency and high energy consumption for normal electrodeposition.[30] Recently, we have found that the micro mixing, mass transfer process and bubble separation rate during composite electrodeposition could be markedly promoted by introducing supergravity field, giving rise to a dramatical change both in the microstructure and the morphology of materials.[20,22,31] Based on the results, this research aims at combining the supergravity field with the

[a]*Hebei Key Laboratory of Applied Chemistry, College of Environmental and Chemical Engineering, Yanshan University, Qinhuangdao 066004, China. E-mail: shaoguangjie@ysu.edu.cn; Fax: +86 335 8061569; Tel: +86 335 8061569*

[b]*State Key Laboratory of Metastable Materials Science and Technology, Yanshan University, Qinhuangdao 066004, China*

† Electronic supplementary information (ESI) available. See DOI: 10.1039/c6ra24993k

‡ Z. Chen and L. Wang contributed equally to this work.

electrodeposition process to acquire Ni–rGO composite cathode with prominently changed morphology and structure for HER. In addition, impacts of both the supergravity field and GO content on the electrocatalytic and physical properties of the composite cathodes were detailedly studied.

2. Experimental

2.1 Preparation of Ni–rGO composite cathodes

The synthesis of Ni–rGO composite cathodes were carried out in the supergravity equipment which has been described detailedly in our previous paper.[32] A ∅ 10 cm × 2 cm copper foil circular ring was used as substrate for composite electrodeposition and a pure nickel pipe was used as anode. All of the copper substrates were mechanically polished, degreased and activated successively before electrodeposition. The Ni–rGO composite cathodes were electrodeposited under various supergravity fields from a nickel sulfamate bath including 350 g L^{-1} $Ni(NH_2SO_3)_2 \cdot 4H_2O$, 10 g L^{-1} $NiCl_2 \cdot 6H_2O$, 30 g L^{-1} NH_4Cl with different contents (0/0.1/0.4/0.7/1.0/1.5 g L^{-1}) of synthesized GO (ESI,† Section 1) in dispersion. The dispersed GO, contacted with the cathode directly, can be electrochemically reduced to form Ni–rGO composite cathodes with the reduced Ni^{2+} (ref. 28, 33 and 34) during the long-time electrodeposition. The electrolyte was continuously sonicated for 60 min before electrodeposition. Various intensities of supergravity fields were achieved by modulating the value of the rotational speed *N*. The composite electrodeposition was executed at a constant current density of 3 A dm^{-2} for 60 min at 318 K.

2.2 Material characterizations

Fourier transform infrared spectroscopy (FT-IR) was performed to analyze the synthesized GO using a Nicolet IS Fourier transformation infrared spectrometer with the wave number range of 500–4000 cm^{-1}. Atomic force microscopy (AFM) was characterized by a commercial instrument (Bruker Multimode 8) to investigate the surface morphologies of GO. TEM image was acquired using an Hitachi HT 7700 field-emission transmission electron microscope operated at 100 kV. The X-ray diffraction (XRD) patterns were recorded on a Rigaku Smart Lab diffractometer with Cu Kα irradiation (λ = 1.5418 Å). The scanning electron microscopy (SEM) measurement was utilized to characterize the morphologies of the composite materials on a Zeiss Supra 55 type field emission scanning electron microscope at an accelerating voltage of 20 kV. The chemical compositional analysis of the composite electrodes was carried out using an energy dispersive spectrometer (EDS) attached to the SEM.

2.3 Electrochemical measurements

The electrochemical measurements were performed in a standard three-electrode cell with 1 M NaOH solution by the CHI 660E electrochemical workstation at room temperature. A platinum foil was used as the counter electrode and an Hg/HgO electrode (0.097 V *vs.* NHE) as the reference electrode. The synthesized circular ring cathode was cutted into several pieces (2 cm × 2 cm) and sealed by insulating epoxy resin, leaving an exposed surface area of 1 cm^2 as the working electrode. Tafel polarization curves were recorded by sweeping the potential from −0.875 to −1.225 V *vs.* Hg/HgO (−0.05 V ≤ η ≤ 0.3 V) at a scan rate of 1 mV s^{-1} to evaluate the HER electrocatalytic activity. IR compensation was performed to correct the polarization data. The electrochemical impedance spectroscopy (EIS) measurements were carried out at a potential of −1.075 V *vs.* Hg/HgO (*i.e.*, an HER overpotential (η) of 150 mV) from 100 kHz to 0.01 Hz with AC voltage amplitude of 5 mV. Cyclic voltammetric (CV) curves were recorded from 0.5 V to −1.5 V *vs.* Hg/HgO with a scan rate of 30 mV s^{-1}. Prior to electrochemical measurements, the working electrodes were activated at a constant current density of 50 mA cm^{-2} for 30 min to remove the oxide film presented on the electrode surface and establish steady state for HER, and the solution was purged with N_2 for 30 min.

3. Results and discussion

Characterization of the synthesized GO sheets was performed by TEM, XRD, AFM and FT-IR measurements (ESI, Section 2 and Fig. S1†). The morphologies of Ni–rGO composite cathodes synthesized under different conditions are presented in Fig. 1. The typical tapered morphology of Ni coating synthesized at rotational speed 3000 rpm is presented in Fig. 1a for comparison. Fig. 1b–d show the morphologies of Ni–rGO cathodes electrodeposited at rotational speed 3000 rpm from the electrolyte including 0.1 g L^{-1}, 0.7 g L^{-1} and 1.5 g L^{-1} GO respectively. It obviously can be observed that the morphologies of Ni–rGO coatings change prominently with rGO sheets appearing in Ni matrix. When the GO concentration adds to 0.7 g L^{-1}, the morphology of composite cathode appears to be a multilayer feature with Ni–rGO hybrid stacking together. It can be seen clearly from the magnified inset as indicated by arrow that the Ni particles with an average size of 300 nm distribute densely and homogeneously on the surface of each rGO sheet to form a sandwich-like structure. However, further enlarging the GO concentration to 1.5 g L^{-1} it comes out to be an aggravation of agglomeration for rGO in Ni matrix as shown in Fig. 1d.

The morphologies of Ni–rGO composite coatings synthesized under various supergravity-field intensities from a same GO concentration of 0.7 g L^{-1} in electrolyte are presented in Fig. 1c and e–g. The inset images are magnified zoom marked by the arrow for each sample. As displayed in Fig. 1e, the catalyst synthesized under normal gravity condition shows a heterogeneous distribution of rGO in matrix, which can be reflected from the accumulational rGO exposing in magnified zoom. However, the uniformly distributed rGO sheets in coatings of Ni–rGO cathodes synthesized at rotational speed 2500, 3000 and 3500 rpm respectively are presented in Fig. 1f, c and g. The EDS elemental mapping of Ni–rGO cathode synthesized at rotational speed 3250 rpm including 0.7 g L^{-1} GO in the bath solution is displayed in Fig. 1h. The elemental mapping images of Ni, C and O illustrate that a portion of oxygenated functional groups in GO remain preserved even after the reduction. The mapping image displays C element is uniformly distributed in

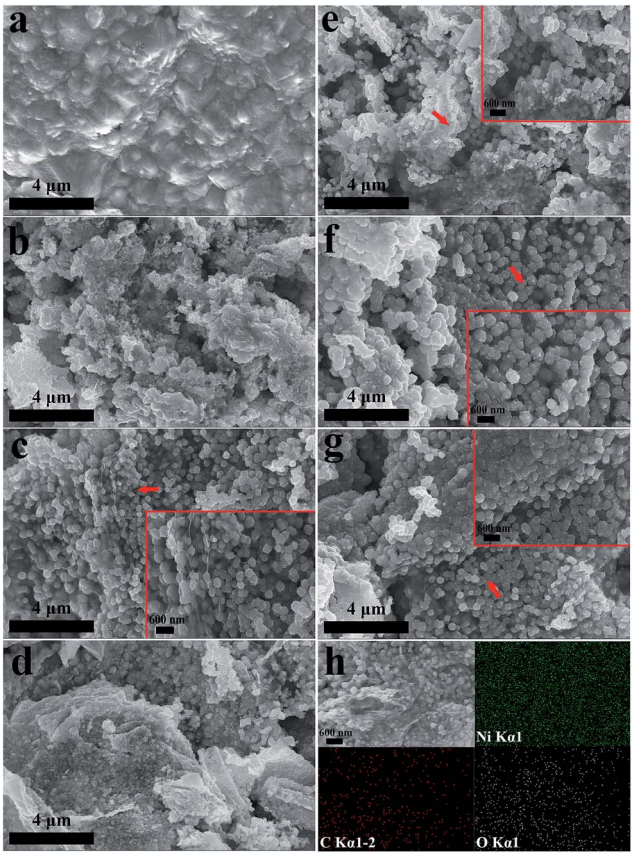

Fig. 1 (a–d) SEM images of Ni–rGO composite cathodes synthesized at different GO concentrations in electrolyte: (a) pure Ni, (b) 0.1 g L^{-1}, (c) 0.7 g L^{-1}, (d) 1.5 g L^{-1}; (e–g) SEM images of Ni–rGO composite cathodes synthesized under different gravity intensities: (e) normal, (f) 2500 rpm, (g) 3500 rpm; (h) EDS elemental mapping of Ni–rGO composite cathode synthesized from 0.7 g L^{-1} GO in solution under rotational speed 3250 rpm. The inset images are magnified zoom marked by the red arrow for each sample.

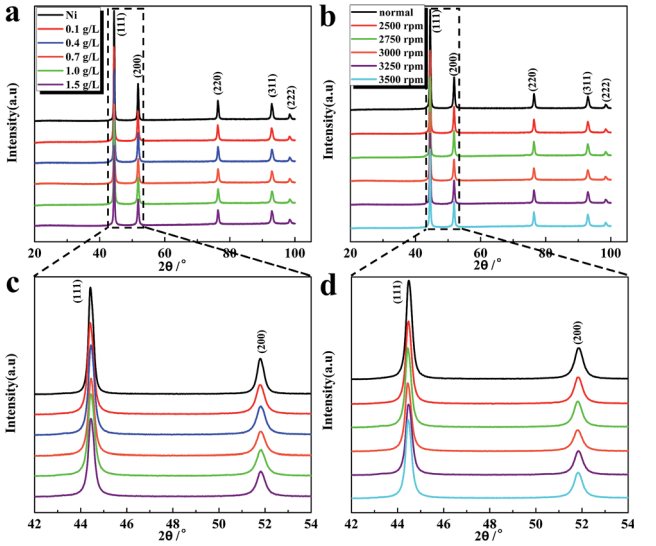

Fig. 2 XRD patterns of (a) Ni–rGO composite cathodes synthesized at various GO concentrations in electrolyte under rotational speed 3000 rpm and (b) Ni–rGO composite cathodes synthesized under various gravity fields from 0.7 g L^{-1} GO in electrolyte; (c) and (d) are the enlarged rectangle regions of (a) and (b), respectively.

the sample, proving that rGO sheets are well embedded in the entire Ni matrix.

The XRD patterns of Ni–rGO catalysts synthesized from various concentrations of GO at a same rotational speed 3000 rpm are presented in Fig. 2a and c. We can find that all the patterns exhibit only diffraction peaks of Ni crystal planes, which is mainly due to the low relative content of rGO embedded in electrode compared with the Ni matrix. It should be noted that the diffraction peaks of Ni become weaken and broader to some extent compared with those in pure Ni coating, especially for the peaks of (111) and (200) of Ni (Fig. 2c), indicating that the Ni grain size in composite cathodes is decreased by introduction of GO during electrodeposition. The fact of grain refinement is a typical phenomenon during composite electrodeposition and can be rationally explained that the rGO incorporated into matrix will not only provide more nucleation sites of Ni crystal seeds but also hinder the coarsening growth of Ni crystal grains.[35,36] As a result, it can be concluded that the difference of morphology between Ni–rGO coating and pure Ni coating should be ascribed to the enhanced nucleation and the retarded crystal growth due to the incorporation of rGO. Fig. 2b and d exhibit the XRD patterns of Ni–rGO composite cathodes synthesized from a same GO concentration of 0.7 g L^{-1} in the electrolyte under various gravity fields. Obviously, each diffraction peak of Ni in the samples synthesized under different intensity of supergravity fields become broader and lower than that of samples synthesized at normal gravity field. It also can be seen more clearly for the peaks of (111) and (200) of Ni in Fig. 3d (magnified rectangle regions of Fig. 2b), demonstrating that the observed grain refinement should be partly attributed to the supergravity fields.

In order to further study the microstructure of catalysts affected by GO concentrations and supergravity intensities, the full width at half maximum (FWHM) of (111) and (200) diffraction peaks of Ni derived from XRD analysis are listed in Table 1. According to the Scherrer's equation which illustrates inverse relation between the crystal size and the FWHM, it can be found from Table 1 that the Ni grain sizes decrease and achieve a minimum value for 0.7 g L^{-1} GO concentration then increase again with the increasing of GO concentration in bath solution (all cathodes are synthesized under the same rotational speed 3000 rpm). This phenomenon has also appeared in our previous research,[22] which can be explained as follows. At the beginning, as the GO concentration improves, more GO sheets tend to be reduced on the cathode surface and introduced into Ni matrix which have the effect of refining crystal sizes. However, further increasing the content of GO in solutions will cause the deterioration of agglomeration for rGO sheets in Ni matrix, resulting in development of coarsening for Ni crystal sizes.

Besides, comparing the FWHM values of the samples synthesized from the same GO concentration (0.7 g L^{-1}) under various gravity fields, it is evident to find that the crystal size of Ni–rGO electrodes synthesized under supergravity fields

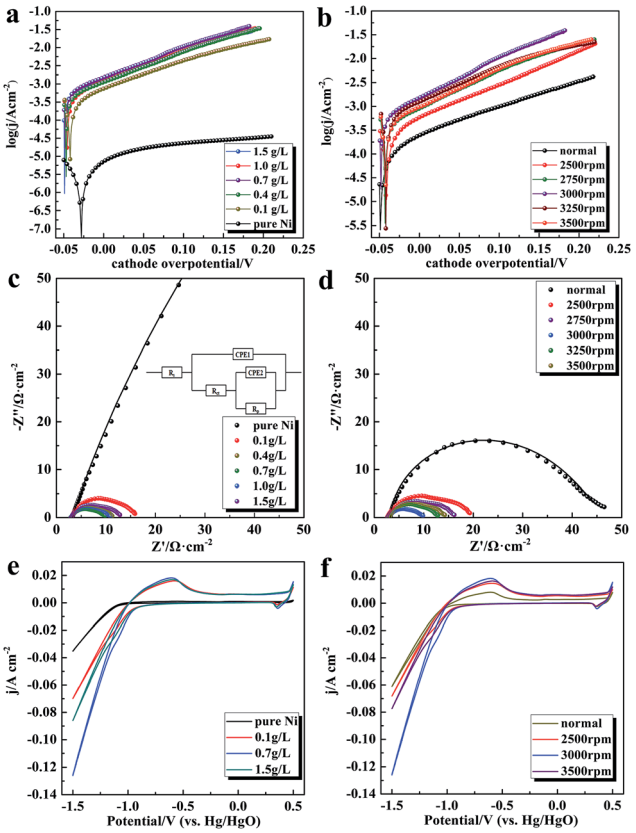

Fig. 3 The electrocatalytic properties for HER in 1.0 M NaOH solution at 298 K on the Tafel curves, Nyquist plots and CV curves of Ni–rGO composite cathodes (a, c and e) synthesized from various GO concentrations in electrolyte under rotational speed 3000 rpm and (b, d and f) synthesized under various gravity fields from 0.7 g L^{-1} GO in electrolyte.

Table 1 FWHM of diffraction peaks Ni (111) and (200) in pure Ni cathode and various Ni–rGO composite cathodes

GO concentration (g L^{-1})	N value (rpm)	$B_{Ni(111)}$ (°)	$B_{Ni(200)}$ (°)
0	3000	0.260	0.363
0.1	3000	0.318	0.448
0.4	3000	0.322	0.457
0.7	Normal	0.307	0.444
0.7	2500	0.319	0.443
0.7	2750	0.323	0.450
0.7	3000	0.329	0.466
0.7	3250	0.334	0.446
0.7	3500	0.327	0.436
1.0	3000	0.334	0.458
1.5	3000	0.322	0.438

decreases obviously, particularly for the samples synthesized at N values of 2750 and 3000 rpm. This phenomenon is primarily attributed to the significant enhancement of supergravity field on the mass transfer and the micro mixing process, promoting the mobility velocity of Ni^{2+} and GO to cathode surface to decrease the concentration polarization and increase the activation polarization. Accordingly, a higher nucleation rate with finer crystal tendency is achieved under supergravity fields. However, it needs to be noted that the grain sizes exhibit a slight coarsening by furthering increasing the N value. Our previous researches have been found that the effective deposition surface area during electrodeposition increases to some degree at higher rotational speed because of the rapid disengagement of H_2 bubbles with lower bubble coverage on cathode surface. Hence, the effective current density for electrodeposition decreases slightly at higher rotational speed, leading to a slight reduction of nucleation rate of Ni crystals.[32,37]

Fig. 3 displays the HER electrocatalytic activities of the synthesized Ni–rGO and pure Ni cathodes. It can be seen from Tafel curves (Fig. 3a) that the Ni–rGO cathodes exhibit prominently enhanced electrocatalytic activities compared to the pure Ni electrode synthesized at the same rotational speed 3000 rpm. As the GO concentration in electrolyte increases to 0.7 g L^{-1}, the electrochemical activity of synthesized Ni–rGO cathode reaches a maximum, and further increasing the content of GO leads to a slight reduction, which means that among the studied range of GO concentration, the content of 0.7 g L^{-1} GO in electrolyte could be regarded as the relatively optimum value. And the degradation of HER activity of Ni–rGO cathodes synthesized under high GO concentration could be mainly attributed to the agglomeration of rGO in Ni matrix. The electrocatalytic performance of the catalysts synthesized under various gravity fields from the same GO concentration of 0.7 g L^{-1} in electrolyte are presented in Fig. 3b. All of the catalysts synthesized under supergravity fields exhibit markedly improved electrocatalytic performance for HER compared with the normal one. Furthermore, the HER performance of the samples increase with the N value enlarging to 3000 rpm, followed by declining as further enhancing the rotational speed. This result also could be ascribed to the coarsening of Ni crystal sizes of composite catalysts synthesized under higher supergravity fields.

The kinetic parameters obtained from the Tafel curves are listed in Table 2. The Ni–rGO composite cathodes yield an evident enhancement on exchange current density j_0 for HER compared with the pure Ni electrode. Among the samples synthesized at same rotational speed 3000 rpm from various GO concentrations, the composite cathode synthesized from the GO content of 0.7 g L^{-1} shows the highest j_0 value of 741.3 μA cm^{-2}. Moreover, all samples synthesized under supergravity fields exhibit higher catalytic activity compared to the one synthesized at normal condition, and the catalyst fabricated at rotational speed 3000 rpm also presents the best performance for HER among the Ni–rGO composite cathodes prepared under different supergravity fields, of which the j_0 value is almost 117 times higher than 6.309 μA cm^{-2} for pure Ni electrode and 5 times higher than 149.6 μA cm^{-2} for the one synthesized under normal gravity field. The current density at overpotential 100 mV of each sample is calculated and denoted as j_{100}. Compared with the pure Ni cathode and Ni–rGO cathode synthesized under normal field, it can be clearly found that all Ni–rGO cathodes synthesized under supergravity fields show higher values. The best Ni–rGO composite cathode produces the highest j_{100} value of 10.7 mA cm^{-2}. This value is superior to the

Table 2 Kinetic parameters obtained from Tafel curves tested in 1 M NaOH solution for HER at 298 K

GO concentration ($g\ L^{-1}$)	N value (rpm)	b ($mV\ dec^{-1}$)	j_0 ($\mu A\ cm^{-2}$)	α	j_{100} ($mA\ cm^{-2}$)
0	3000	185	6.309	0.32	2.3×10^{-2}
0.1	3000	128	346.7	0.46	4.5
0.4	3000	121	537.0	0.49	7.8
0.7	Normal	160	149.6	0.37	1.0
0.7	2500	142	331.1	0.42	2.8
0.7	2750	124	436.5	0.48	5.6
0.7	3000	120	741.3	0.49	10.7
0.7	3250	132	630.9	0.45	6.9
0.7	3500	125	467.7	0.47	6.0
1.0	3000	115	575.4	0.51	8.9
1.5	3000	128	512.9	0.46	9.1

values of some other Ni and Ni-based alloys cathodes published recently, including Ni nanospike arrays ($j_{300} \sim 10\ mA\ cm^{-2}$, 1 M KOH),[38] $Ni_{0.95}Sm_{0.05}$ alloy ($j_{200} \sim 5\ mA\ cm^{-2}$, 8 M KOH),[39] NiW alloy ($j_{250} \sim 10\ mA\ cm^{-2}$, 6 M KOH)[12] and Pd–Ni–Mo film ($j_{280} \sim 10\ mA\ cm^{-2}$, 1 M NaOH).[40] The superior catalytic performance of Ni–rGO cathodes synthesized under supergravity fields could be attributed to the following reasons: (1) the unique multilayer structure with large numbers of Ni nanoparticles anchoring on the rGO surface has significantly increased the surface area and provided more active sites for H adsorption during the Volmer step; (2) the cooperative effect between the Ni nanoparticles and the rGO sheets facilitates the H_{ads} spillover from the Ni particles surface and migrate onto the rGO surface to enable the cleaning of Ni particles surface with more free active sites for H_{ads} to be formed.[27]

Tafel slope b also can estimate the HER mechanism for the electrodes, and the HER process have summarized as the following three essential steps: (1) the Volmer reaction: $M + H_2O + e^- = M\text{–}H_{ads} + OH^-$ ($b = 120$ mV), (2) the Heyrovsky reaction: $M\text{–}H_{ads} + H_2O + e^- = M + H_2 + OH^-$ ($b = 40$ mV), and/or (3) the Tafel reaction: $2M + H_{ads} = 2M + H_2$ ($b = 30$ mV). As listed in Table 2, most of the Tafel slopes of Ni–rGO composite cathodes synthesized under supergravity fields are $\sim 120\ mV\ dec^{-1}$, which can be inferred that the rate-determining step of HER may be the Volmer step or the Volmer step coupled with one of the other two steps.[19] However, it is noteworthy that the Tafel slopes of Ni–rGO cathodes synthesized under supergravity fields all turn out to be slight increase at higher overpotentials as shown in Fig. 3a and b. This phenomenon has also been reported by other researchers before and could be related to the formation of hybrids in the cathode surface. As the overpotentials increase, a large number of H_{ads} and H_2 are generated and adsorbed on the cathode surface, which gradually becomes a barrier to modify the electronic and structural state of the cathode/electrolyte interface, causing the slight increase in the Tafel slopes.[41–44] Noticeably, it has been found that the Ni–rGO composite cathodes synthesized under supergravity fields in this paper display more active behaviors than our previous researches and also some other recently reported works on Ni-based catalysts (Table S1†).

In order to further analyze the electrochemical behaviors on the composite electrodes, EIS measurements are performed at cathode overpotential of 150 mV and the corresponding complex plane Nyquist plots are shown in Fig. 3c and d (symbols were experimental data and solid lines were fitted curves). The impedance spectra are characterized by the Armstrong's equivalent electric circuit model based on the single-adsorbate mechanism as depicted in the inset of Fig. 3c.[45] The relevant parameters simulated from the EIS spectra are displayed in Table S2.† Compared with the pure Ni cathode, it can be seen that both R_{ct} and R_p values of Ni–rGO cathodes decrease drastically. As we know, the smaller value of R_{ct} illustrates more favorable for the Volmer reaction during HER process. The R_{ct} of composite cathodes synthesized at the same rotational speed 3000 rpm shows a minimum value of 5.47 $\Omega\ cm^{-2}$ for the sample synthesized from 0.7 $g\ L^{-1}$ GO in electrolyte, which is also the lowest among those of Ni–rGO samples synthesized at various supergravity intensities. It is almost 87 and 7 times lower than those of pure Ni cathode and Ni–rGO cathode synthesized at normal field, respectively. The above results are in keeping with Tafel analysis, and it is in depth confirmed that the best electrochemical behavior for HER of Ni–rGO cathodes was synthesized under supergravity field of rotational speed 3000 rpm with optimal GO concentration of 0.7 $g\ L^{-1}$ in electrolyte. The value of $(R_{ct} + R_p)$ could also explain electrocatalytic activity for HER which have studied in our published papers.[18,20]

Considering electrochemical active surface area plays a crucial role in improving electrocatalytic activity for HER, the surface roughness R_f is calculated by comparing the double layer capacitance C_{dl} value with 20 $\mu F\ cm^{-2}$ for smooth electrode surface ($R_f = C_{dl}/20$).[44] The double layer capacitance C_{dl} of the electrode is obtained by using the equation from Brug *et al.*[10,46–49] As calculated in Table 3, it can be found that the R_f values of Ni–rGO composite samples increase remarkably compared with the pure Ni electrode, and obtain the highest value of 836 for 0.7 $g\ L^{-1}$ GO in bath solution. Furthermore, all R_f values of composite cathodes synthesized under supergravity fields are enhanced obviously compared to the sample synthesized at normal condition. The higher R_f value means providing more electrocatalytic active sites at per unit apparent surface area for HER, which is mainly ascribed to the multilayer sandwich-like structure of Ni–rGO composite with large numbers of nano-sized Ni particles growing on. In addition, it is a good way to compare the intrinsic activity of the electrodes through normalizing the current densities to R_f at overpotential of 100 mV (*i.e.* j_{100}/R_f) as presented in Table 3. At the overpotential of 100 mV, the average value of j_{100}/R_f for the catalysts synthesized under supergravity fields is about 3 times higher than the values of the pure Ni cathode and the normal one. It means that the intrinsic activity of Ni–rGO composite cathodes synthesized under supergravity fields increases significantly compared with the Ni–rGO cathode synthesized under normal condition and the pure Ni cathode. The improved intrinsic activity of the catalysts should be mainly ascribed to the promoted cooperative effect between the Ni nanoparticles and the well-integrated rGO sheets by the unique multilayer structure.

Table 3 Relevant electrochemical parameters calculated from the fitting EIS data

GO concentration ($g\ L^{-1}$)	N value (rpm)	C_{dl} ($mF\ cm^{-2}$)	R_f	j_{100}/R_f ($\mu A\ cm^{-2}$)
0	3000	0.097	5	4.60
0.1	3000	8.067	403	11.17
0.4	3000	10.90	547	14.26
0.7	Normal	4.257	213	4.69
0.7	2500	5.839	292	9.59
0.7	2750	8.201	410	13.66
0.7	3000	16.70	836	12.80
0.7	3250	9.899	495	13.94
0.7	3500	8.334	417	14.39
1.0	3000	14.20	710	12.53
1.5	3000	8.612	431	21.11

CV curves of Ni–rGO composite cathodes synthesized under various gravity fields were researched in alkaline solution at a scan rate of 30 mV s^{-1} between 0.5 V and −1.5 V. As exhibited in Fig. 3e, the CV plots of all Ni–rGO cathodes show obvious reduction peaks at the potential range of −1.1 V to −1.0 V and oxidation peaks at −1.0 V to −0.5 V (*vs.* Hg/HgO), which are associated with the H atoms adsorption process and the oxidation of Ni to $NiO/Ni(OH)_2$ respectively.[39,50] It can be observed in Fig. 4a that the curve of pure Ni electrode displays a low peak cathodic current density (i_{pc}) with small area covered under CV plots, suggesting poor catalytic performance for HER. The curves of Ni–rGO cathodes present significant enhancement in the i_{pc} values and the area covered under CV curves, revealing higher electrochemical active surface area coupled with activation process of H atoms adsorbed/desorbed on the cathodes surface especially for the sample synthesized from 0.7 g L^{-1} GO in solution, which is in line with the results revealed in above EIS measurement. As displayed in Fig. 3f, the CV curves of Ni–rGO composite cathodes synthesized under different supergravity fields present both higher i_{pc} and larger area covered under CV curves than that of prepared under normal condition. In accordance with the results found in Tafel and EIS measurements, the Ni–rGO composite cathode synthesized at rotational speed 3000 rpm shows a more favorable catalytic activity for HER. It is mainly due to the unique multilayer structure of like sandwich and larger active surface area of the composite electrodes.

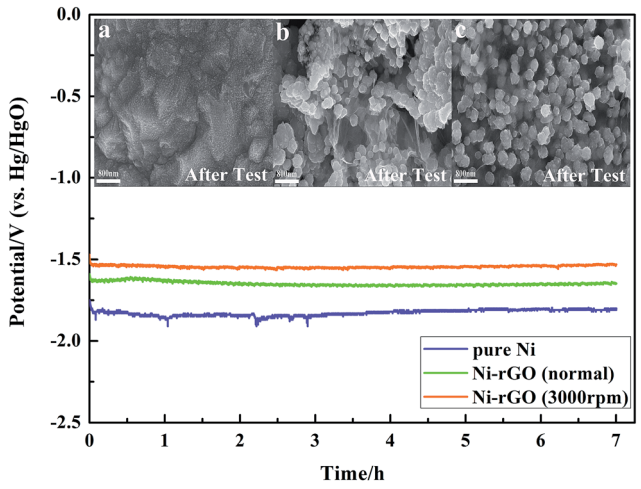

Fig. 4 Chronopotentiometry curves of Ni and Ni–rGO cathodes tested at 250 mA cm^{-2} for 7 h in 1 M NaOH solution. The inset images display the morphology after tested of (a) pure Ni electrode, (b) Ni–rGO cathode synthesized under normal gravity field, (c) Ni–rGO cathode synthesized under rotational speed 3000 rpm.

The performance of stability during the long-term electrolysis is another essential criteria to evaluate the cathode materials for practical utility. Therefore, chronopotentiometry test for a consecutive HER on the synthesized Ni and Ni–rGO cathodes were tested under a constant current density of 250 mA cm^{-2} (*i.e.* the current density normally used in industrial operation) for 7 h in the same configuration. It can be seen in Fig. 4 that the curves of all studied samples display a declined process of potential in the initial period due to the reduction of the oxides on the cathodes surface and then gradually tend to smooth and steady. The pure Ni electrode shows a higher cathodic potential and more unstable electrolysis during the long-term HER, which results from the collapse of Ni-based structure and interference by the adsorption/desorption of big H_2 bubbles on the cathode surface. Compared to the pure Ni electrode, the Ni–rGO cathode synthesized under normal gravity field displays apparent enhancement on the HER stability, yet still shows a higher cathodic potential than the Ni–rGO composite catalyst synthesized under rotational speed 3000 rpm, which presents a good electrochemical stability with the minimum potential for HER. The above results are in agreement with the else electrochemical measurements. During the stabilized electrolysis process, the Ni–rGO cathode synthesized under rotational speed 3000 rpm undergoes negligible deterioration in cathodic potential, revealing that it has robust durability and stability for long-time HER. The surface morphologies of three catalysts after long-time HER were studied and revealed in the inset of Fig. 4. Evidently, a large number of spots appear on the surface of pure Ni electrode, compared with the pristine morphology in Fig. 1a, prevailingly caused by the alkaline corrosion and H_2 impulsion. However, surface morphologies of Ni–rGO composite cathodes both present almost no change after chronopotentiometry testing, declaring that the incorporation of graphene sheets in composite cathodes can effectively defend against the aggressive alkaline solution and improve the stability of electrode materials.

Based on the systematic analysis, it confirms that the Ni–rGO cathode synthesized with 0.7 g L^{-1} GO in bath at rotational speed 3000 rpm shows the best catalytic performance and stability for HER in 1 M NaOH solution. The excellent HER performance could be ascribed to the unique morphology feature of the composite cathodes which is benefited from the utilization of supergravity fields. The remarkably improved mass transfer and micro mixing process under supergravity fields can facilitate the disengagement of hydrogen bubbles from electrode surface timely and accelerate the transfer of GO sheets towards cathode to be reduced. Thus, the embedded rGO sheets will act as the new substrates for Ni^{2+} being reduced on

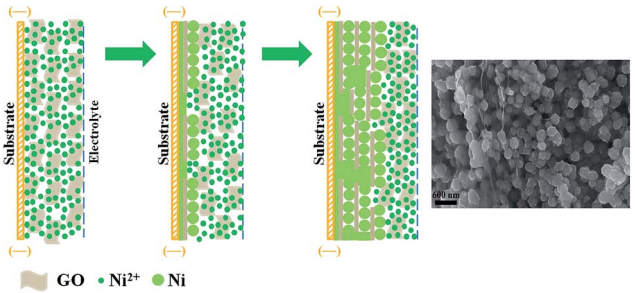

Fig. 5 Schematic illustration of the formation process of Ni–rGO composite cathode synthesized under supergravity field.

its surface to form *in situ* growing nano-sized Ni particles. As the electrodeposition process continuous, the Ni–rGO hybrid stacked one by one gives rise to the sandwich-like hierarchical structure. In addition, the interspace between the stacked Ni–rGO hybrid can provide an easy path for electrolyte diffusing in, which ensures the formation of more nano-sized Ni particles between the interlayers during electrodeposition process. This unique multilayer structure with numerous Ni nanoparticles anchoring on the rGO surface has greatly increased the active surface area and effectively enhanced the cooperative effect between Ni nanoparticles and rGO sheets. Hence, the Ni–rGO cathode synthesized under the optimum GO concentration and supergravity strength shows outstanding electrocatalytic property for HER. The schematic illustration of the proposed behaviors of Ni^{2+} and GO under supergravity fields during electrodeposition is given in Fig. 5, which provides a visual description for the structure evolution.

4. Conclusions

In summary, we have synthesized the Ni–rGO composite cathode with a new hierarchical morphology through a single step method of electrodeposition under supergravity field. Such morphology feature coupled with large numbers of nano-sized Ni particles provides high active surface area for HER and ensures a favorable cooperative effect between the rGO sheets and Ni to facilitate the H_{ads} migrate from the Ni particles to rGO surface. The electrochemical testings present that the catalytic performance of Ni–rGO composite cathodes are enhanced prominently compared with that synthesized under normal gravity field. The sample synthesized at rotational speed 3000 rpm from the optimal GO concentration 0.7 g L^{-1} achieves the highest exchange current density for HER, which is about 117 times and 5 times higher than that on pure Ni cathode and Ni–rGO cathode synthesized under normal gravity condition respectively. During the long-term HER test, the composite cathode exhibits excellent stability with almost unchanged morphology feature.

Acknowledgements

This work was financially supported by the National Natural Science Foundation of China (No. 51674221).

Notes and references

1 H. B. Gray, *Nat. Chem.*, 2009, **1**, 7.
2 M. Dresselhaus and I. Thomas, *Nature*, 2001, **414**, 332–337.
3 J. A. Turner, *Science*, 2004, **305**, 972–974.
4 K. Zeng and D. Zhang, *Prog. Energy Combust. Sci.*, 2010, **36**, 307–326.
5 M. G. Walter, E. L. Warren, J. R. McKone, S. W. Boettcher, Q. Mi, E. A. Santori and N. S. Lewis, *Chem. Rev.*, 2010, **110**, 6446–6473.
6 B. Conway and B. Tilak, *Electrochim. Acta*, 2002, **47**, 3571–3594.
7 W. Sheng, H. A. Gasteiger and Y. Shao-Horn, *J. Electrochem. Soc.*, 2010, **157**, B1529–B1536.
8 M. Gong, D.-Y. Wang, C.-C. Chen, B.-J. Hwang and H. Dai, *Nano Res.*, 2016, **9**, 28–46.
9 P. Los, A. Rami and A. Lasia, *J. Appl. Electrochem.*, 1993, **23**, 135–140.
10 N. Krstajić, V. Jović, L. Gajić-Krstajić, B. Jović, A. Antozzi and G. Martelli, *Int. J. Hydrogen Energy*, 2008, **33**, 3676–3687.
11 C. Lupi, A. Dell'Era and M. Pasquali, *Int. J. Hydrogen Energy*, 2009, **34**, 2101–2106.
12 S. H. Hong, S. H. Ahn, J. Choi, J. Y. Kim, H. Y. Kim, H.-J. Kim, J. H. Jang, H. Kim and S.-K. Kim, *Appl. Surf. Sci.*, 2015, **349**, 629–635.
13 Y. Zhu, X. Zhang, J. Song, W. Wang, F. Yue and Q. Ma, *Appl. Catal., A*, 2015, **500**, 51–57.
14 I. Paseka, *Electrochim. Acta*, 2001, **47**, 921–931.
15 Q. Han, K. Liu, J. Chen and X. Wei, *Int. J. Hydrogen Energy*, 2003, **28**, 1207–1212.
16 T. V. Vineesh, S. Mubarak, M. G. Hahm, V. Prabu, S. Alwarappan and T. N. Narayanan, *Sci. Rep.*, 2016, **6**, 31202.
17 N. Krstajić, U. Lačnjevac, B. Jović, S. Mora and V. Jović, *Int. J. Hydrogen Energy*, 2011, **36**, 6450–6461.
18 L. Vázquez-Gómez, S. Cattarin, P. Guerriero and M. Musiani, *Electrochim. Acta*, 2007, **52**, 8055–8063.
19 D. A. Dalla Corte, C. Torres, P. dos Santos Correa, E. S. Rieder and C. de Fraga Malfatti, *Int. J. Hydrogen Energy*, 2012, **37**, 3025–3032.
20 Z. Chen, Z. Ma, J. Song, L. Wang and G. Shao, *RSC Adv.*, 2016, **6**, 60806–60814.
21 Z. Zheng, N. Li, C.-Q. Wang, D.-Y. Li, F.-Y. Meng and Y.-M. Zhu, *J. Power Sources*, 2013, **222**, 88–91.
22 Z. Chen, Z. Ma, J. Song, L. Wang and G. Shao, *J. Power Sources*, 2016, **324**, 86–96.
23 A. K. Singh, M. A. Ribas and B. I. Yakobson, *ACS Nano*, 2009, **3**, 1657–1662.
24 Y. Gao, N. Zhao, J. Li, E. Liu, C. He and C. Shi, *Int. J. Hydrogen Energy*, 2012, **37**, 11835–11841.
25 K. Spyrou, D. Gournis and P. Rudolf, *ECS J. Solid State Sci. Technol.*, 2013, **2**, M3160–M3169.
26 L. Wei and Y. Mao, *Int. J. Hydrogen Energy*, 2016, **41**, 11692–11699.
27 D. Chanda, J. Hnát, A. S. Dobrota, I. A. Pašti, M. Paidar and K. Bouzek, *Phys. Chem. Chem. Phys.*, 2015, **17**, 26864–26874.
28 D. Kuang, L. Xu, L. Liu, W. Hu and Y. Wu, *Appl. Surf. Sci.*, 2013, **273**, 484–490.

29 M. Khalil, T. A. S. Eldin, H. Hassan, K. El-Sayed and Z. A. Hamid, *Surf. Coat. Technol.*, 2015, **275**, 98–111.
30 M. Wang, Z. Wang, X. Gong and Z. Guo, *ChemElectroChem*, 2015, **2**, 1879–1887.
31 S. Liu, Y. Liu, W. Song, J. Song, C. Wang, G. Shao and X. Qin, *J. Solid State Electrochem.*, 2015, **19**, 1321–1329.
32 J. Du, G. Shao, X. Qin, G. Wang, Y. Zhang and Z. Ma, *Mater. Lett.*, 2012, **84**, 13–15.
33 L. Chen, Y. Tang, K. Wang, C. Liu and S. Luo, *Electrochem. Commun.*, 2011, **13**, 133–137.
34 Z. Pu, Q. Liu, A. M. Asiri, A. Y. Obaid and X. Sun, *J. Power Sources*, 2014, **263**, 181–185.
35 C. P. Kumar, T. Venkatesha and R. Shabadi, *Mater. Res. Bull.*, 2013, **48**, 1477–1483.
36 B. Praveen and T. Venkatesha, *J. Alloys Compd.*, 2009, **482**, 53–57.
37 Z. Chen, G. Shao, Z. Ma, J. Song, G. Wang and W. Huang, *Mater. Lett.*, 2015, **160**, 34–37.
38 H. Ogihara, M. Fujii and T. Saji, *RSC Adv.*, 2014, **4**, 58660–58663.
39 D. Cardoso, L. Amaral, D. Santos, B. Šljukić, C. Sequeira, D. Macciò and A. Saccone, *Int. J. Hydrogen Energy*, 2015, **40**, 4295–4302.
40 J. Tang, X. Zhao, Y. Zuo, P. Ju and Y. Tang, *Electrochim. Acta*, 2015, **174**, 1041–1049.
41 J. Highfield, E. Claude and K. Oguro, *Electrochim. Acta*, 1999, **44**, 2805–2814.
42 M. Metikoš-Huković and A. Jukić, *Electrochim. Acta*, 2000, **45**, 4159–4170.
43 R. Šimpraga, G. Tremiliosi-Filho, S. Qian and B. Conway, *J. Electroanal. Chem.*, 1997, **424**, 141–151.
44 E. Navarro-Flores, Z. Chong and S. Omanovic, *J. Mol. Catal. A: Chem.*, 2005, **226**, 179–197.
45 R. Armstrong and M. Henderson, *J. Electroanal. Chem.*, 1972, **39**, 81–90.
46 G. Brug, A. Van Den Eeden, M. Sluyters-Rehbach and J. Sluyters, *J. Electroanal. Chem.*, 1984, **176**, 275–295.
47 M. Wang, Z. Wang, X. Yu and Z. Guo, *Int. J. Hydrogen Energy*, 2015, **40**, 2173–2181.
48 C. González-Buch, I. Herraiz-Cardona, E. Ortega, J. García-Antón and V. Pérez-Herranz, *Int. J. Hydrogen Energy*, 2013, **38**, 10157–10169.
49 F. Rosalbino, G. Scavino and M. A. Grande, *J. Electroanal. Chem.*, 2013, **694**, 114–121.
50 E. A. Franceschini, G. I. Lacconi and H. R. Corti, *Electrochim. Acta*, 2015, **159**, 210–218.